

# Limit Cycles, Noise, and Chaos in Hearing

R. STOOP,<sup>1,2\*</sup> J.-J. V.D. VYVER,<sup>1</sup> AND A. KERN<sup>1</sup>

<sup>1</sup>*Institute of Neuroinformatics ETHZ/UNIZH, CH-8057 Zürich-Irchel, Switzerland*

<sup>2</sup>*University of Applied Sciences Northwestern Switzerland, Solothurn  
4600 Olten, Switzerland*

**KEY WORDS** limit cycles; bifurcations; noise; chaos; stochastic resonance; neural coding; variability

**ABSTRACT** Based on insight obtained from a newly developed cochlea model, we argue that noise-driven limit cycles are the basic ingredient in the mammalian cochlea hearing process. For insect audition, we provide evidence in favor of the persistence of this principle. We emphasize the role of bifurcations for the emergence of broad-range sound perception, both in the frequency and amplitude domain, and indicate that this crucially depends on the correct coupling between limit cycles. We review the limit-cycle coupling universality, and outline how it can be used to encode information. Cortical noise is the microscopic basis for this encoding, whereas chaos emerges as the macroscopic expression of computation being done in the network. Large neuron firing variability is one possible consequence of the proposed mechanism that may apply to both vertebrate and insect hearing. *Microsc. Res. Tech.* 63:400–412, 2004. © 2004 Wiley-Liss, Inc.

## BIFURCATIONS AND LIMIT CYCLES IN THE MAMMALIAN COCHLEA

Since the advent of the computer age, investigations of dynamical processes are no longer restricted to linear models. As a consequence, during the last decades, nonlinear dynamical systems theory became a success story. Using notions and concepts from this field, the effects of the nonlinearities were investigated in detail, revealing, in addition to the notion of a fixed point known from linear theory, the importance of novel types of invariant objects. These more general objects are limit cycles and chaotic attractors, where chaos can be regarded as being composed of limit cycles that have become unstable. In this way, the latter still dictate the general appearance and properties of a chaotic attractor. Before these limit cycles permanently get unstable (i.e., for an interval of the control parameter space that has a non-zero measure), they once in a while undergo a bifurcation, where they generally change their periodicity in a period-doubling manner (pitchfork-bifurcation, Feigenbaum scenario; Feigenbaum, 1978). Between the occurrence of bifurcations, limit cycles are generally very stable. An interesting engineering point of view is that in this state, they convert an analog control parameter into an integer-valued periodicity. Close to the bifurcation points, they have another attractive property: They can serve as small signal amplifiers (Derighetti et al., 1985; Wiesenfeld and McNamara, 1985). The sensitivity of the human cochlea, and possibly that of some insect hearing organs, to small signal input can be considered as a direct consequence of this property.

In the auditory system of many vertebrate species, receptor cells show the phenomenon of resonance upon appropriate sensory stimulation. Hair cells in the cochlea, which are placed tonotopically along the basilar membrane, are activated by mechanically sensitive cilia, which modulate the conductance of their membrane. Upon a step current stimulation, the membrane

potential responds with an exponentially damped oscillation, where the frequency close to the resting potential is the one that the cell is most sensitive to (Crawford and Fettiplace, 1983). At the onset, the cell displays the characteristics of a Hopf bifurcation, whose main property is a nonlinear amplification. In our recently developed mammalian cochlea model (Kern et al., 2002), this important aspect of nonlinear signal processing is biomorphically implemented for the first time. As it may also serve as a guideline for the understanding of insect hearing, the model will be outlined below in some detail.

Cochlear modelling has a long tradition, starting with the first model by H.L.F. Helmholtz in 1863. More recently, von Békésy's discovery of traveling waves along the basilar membrane (BM) (see, e.g., von Békésy, 1960) gave rise to passive hydrodynamic models (de Boer, 1980; Lighthill, 1981). Already in 1948, Gold conjectured that in the cochlea an active mechanism must be present (Gold, 1948). Evidence for this property was furnished by the discovery in 1978 of oto-acoustic emissions, i.e., the fact that the ear is itself able to produce sounds (Kemp, 1978). In the following years, various experiments revealed that the outer hair cells (OHC), which reside on top of the basilar membrane, are the source of active amplification (see Eguíluz et al., 2000).

In Eguíluz et al. (2000), it was advocated that the compression of the dynamic range, sharper tuning for softer sounds, and generation of combination tones, are fingerprints of Hopf bifurcations. Our modeling assumption, for which there now is growing experimental

\*Correspondence to: R. Stoop, Institute of Neuroinformatics ETHZ/UNIZH, Winterthurerstr. 190, CH-8057 Zürich-Irchel, Switzerland.  
E-mail: ruedi@ini.phys.ethz.ch

Received 19 May 2003; accepted in revised form 20 September 2003

DOI 10.1002/jemt.20055

Published online in Wiley InterScience (www.interscience.wiley.com).

evidence (Martin et al., 2001), is that the outer hair cells (OHC) determine the active amplification and are the source of the Hopf behavior. The Hopf differential equation reads

$$d/dt z(t) = (\mu + i\omega_0)z - |z|^2z + Fe^{i\omega t}, \quad (1)$$

where the last term constitutes an external periodic forcing with frequency  $\omega$ ,  $z(t)$  is complex,  $\omega_0$  is the natural frequency of the oscillation, and  $\mu$  denotes the real-valued control parameter. We will show now that cochlear hearing properties can be precisely reproduced by a careful biomorphic implementation of Hopf amplifiers. Hopf bifurcators are easily implemented in biochemistry as well as in silicon.

If we choose  $F = 0$  (no external driving), (1) corresponds to the generic differential equation of a system displaying a Hopf bifurcation. For  $\mu < 0$ , the solution  $z(t) = 0$  is a stable fixed point, while for positive  $\mu$  the fixed-point solution becomes unstable and a stable limit cycle  $z(t) = \mu^{1/2} e^{i\omega_0 t}$  appears (the so-called Hopf bifurcation, see Hopf, 1942).

In the presence of a forcing  $F(t) = F e^{i\omega t}$ , the corresponding  $z(t)$  is the amplified signal. For periodic forcing, assuming 1:1-locking between the input and the response, the steady state solution is obtained by the ansatz  $z(t) = R e^{i\omega t + i\phi}$  (for sinusoidal stimuli at moderate intensities, where the cochlea behaves highly nonlinear, no higher harmonics are generated).  $R$  can then be determined by the bi-cubic equation

$$F^2 = R^6 - 2\mu R^4 + [\mu^2 + (\omega - \omega_0)^2]R^2. \quad (2)$$

For  $\mu = 0$  and close to resonance  $\omega = \omega_0$ ,  $R = F^{1/3}$ . As  $F$  tends towards zero, the gain  $G = R/F = F^{-2/3}$  increases infinitely. Hence, the response of the system is compressively nonlinear. For  $\mu < 0$ ,  $\omega = \omega_0$  and weak stimuli, it is obtained that  $R = -F/\mu$ . When  $F$  is increased, the term  $R^6$  can no longer be neglected, and, as  $R^6 \sim \mu^2 R^2$ , the compressive nonlinear regime is entered (the transition occurring at about  $F = (-\mu)^{3/2}$ ). Therefore, for weak stimuli  $F$  of a given frequency, the response  $R$  is nearly linear, while for moderate stimuli, the differential gain  $dR/dF$  decreases with increasing stimulus intensity. Away from the resonance, the last term in (2) dominates, so that  $R \sim F/|\omega - \omega_0|$ , which yields a linear response, for every kind of input. Past the bifurcation point ( $\mu > 0$ ), stable limit-cycles emerge.

### Passive Cochlea Behavior

The cochlear fluid is considered incompressible and inviscid (de Boer, 1980), and, as the BM displacements are small ( $\mu\text{m}$ -range), a linear theory of the passive components is justified. This assumption is well supported by experiments: For intense sounds, where active amplification is essentially turned off, linear BM input-output functions are observed. The passive BM, therefore, performs sinusoidal movements (nonlinear behavior will later be entirely attributed to the active process). This situation can be shown to be equivalent to a water wave (Patuzzi, 1996), where the surface is loaded with a mass density  $m$  and an exponentially decreasing transversal stiffness  $E(x)$ , given by

$$E(x) = E_0 e^{-\alpha x}, \quad (3)$$

where  $x$  is the distance along the BM. Physiological measurements reveal that longitudinal coupling along the BM, which leads to a non-vanishing surface tension, is small. For a mass-loaded stiff water surface, the dispersion relation can be derived by linearizing the boundary conditions of the Laplace equation, leading to

$$k(x, \omega) \tanh(k(x, \omega)h) = \rho\omega^2/(E(x) - m\omega^2), \quad (4)$$

where  $k = 2\pi/\lambda$  is the wave vector,  $h$  is the radius of the cochlear duct, and  $\rho$  is the fluid density. If the characteristic frequency at location  $x$  is denoted by  $\omega_c(x)$ , it is evident that  $k(x, \omega)$  diverges as  $\omega \rightarrow \omega_c(x)$ .

For the determination of the energy density distribution along the cochlear duct, the dependence of the group velocity  $v_G$  on  $x$  is of importance. From (4), it is found that as the tonotopic location of the particular frequency  $\omega_c$  is approached,  $v_G \rightarrow 0$ . This means that the traveling wave stalls at the point of (passive) resonance, where its wavelength decays to zero, and, as a consequence, in the absence of dissipation, energy density and wave amplitude diverge.

Given an energy density  $e_0 = e(x = 0)$  at the basal end of the cochlea, the energy propagates with group velocity. Then, the steady-state distribution of the one-dimensional energy density  $e(x)$  along the cochlear duct is given by

$$e(x, \omega) = e_0(x, \omega) \frac{v_G(0, \omega)}{v_G(x, \omega)} \exp\left(-\int_0^x \frac{d(y, \omega)}{v_G(y, \omega)} dy\right) \quad (5)$$

where  $d$  measures the hydrodynamic attenuation. Noting that the kinetic and the potential energy, averaged over one cycle, contribute equally to total energy, the BM displacement amplitude  $A(x, \omega)$  is obtained as

$$A(x, \omega) = (2e(x, \omega)/E(x))^{1/2}. \quad (6)$$

An example of a passive response curve is given by the dashed line in Figure 1a. It is instructive to compare our model to the excitation patterns obtained by De Boer's one-dimensional model (de Boer, 1990), where the Laplace equation is directly solved using the WKB approximation method. In the long wave limit, the response of this model grows as  $\exp(3/4 \alpha x)$ . In our model, this behavior is directly seen from the long-wave approximation of  $e(x, \omega)$ , using (6).

### Active Amplification

Active amplification, generated by Hopf oscillators residing in the array of outer hair cells, is described by a local supply of energy  $a(\cdot)$  injected into the hydrodynamic wave. An observer moving with the traveling wave observes the gain

$$\partial e(x, t)/\partial t|_{\text{act}} = a(x, \omega, e(x, t)), \quad (7)$$

leading to the differential equation

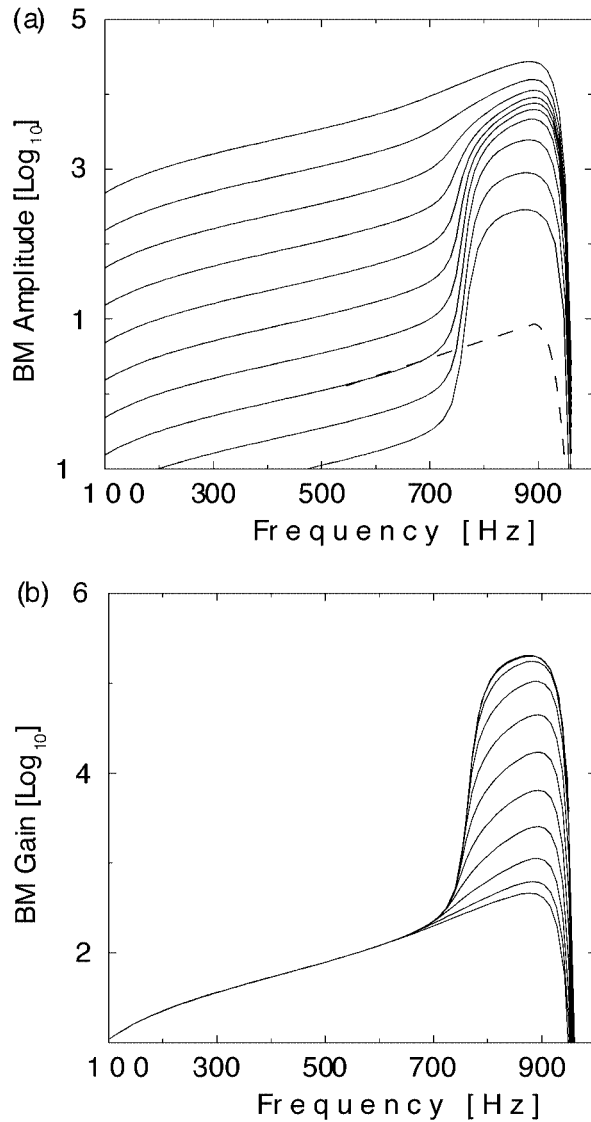


Fig. 1. Local BM response from an array of Hopf bifurcators, no coupling. **a**: Frequency response of the BM at  $x_c(\omega = 1,000 \text{ Hz})$ ; dashed line: frequency response of the passive model. **b**: Gain of the BM, relative to vibration at the oval window.

$$\frac{\partial e}{\partial \mathbf{x}} = -\frac{1}{v_G(\mathbf{x}, \omega)} \left[ \frac{\partial v_G}{\partial \omega}(\mathbf{x}, \omega) + d(\mathbf{x}, \omega) \right] e(\mathbf{x}, \omega) + \frac{a(e(\mathbf{x}, \omega), \mathbf{x}, \omega)}{v_G(\mathbf{x}, \omega)} \quad (8)$$

The explicit form of the term  $a(\cdot)$  is deduced from the driven Hopf system

$$d/dt z(t) = (\mu + i\omega_{ch})z - \gamma|z|^2z + Fe^{i\omega t}, \quad (9)$$

by imposing a biophysically justified relation between the input signal  $F$  and the stationary response amplitude  $R$  of the amplifier (see Eq. (2)), to the local energy density  $e$ . Parameter  $\gamma$  is used to rescale different mag-

nitudes of  $(F, R)$ , but does not introduce an additional degree of freedom into the system.

The dependence of  $F$  and  $R$  on  $e$  reveals clear interpretations of the emergent modeling parameters  $\sigma(\omega)$  and  $K(\omega)$ . After having fixed  $\gamma$  for all occurring frequencies  $\omega$ , the transition point  $e_{cnl}(\omega)$  is set by  $\sigma(\omega)$  for each  $\omega$ . The corresponding  $K(\omega)$  then determines the gain. It can be shown that the two functions can be approximated by a simple exponential rule, depending only on the stiffness exponent  $\alpha$  [see (3)] and on the Hopf control parameter  $\mu$ , which sets the amplifier's bandwidth.

At this point, the model has a minimal number of 4 free parameters, valid for the whole frequency range. Moreover, to each of the parameters, a clear interpretation in terms of the model response is attached, which allows easy modifications of the output. Figure 1 shows frequency response and gain of the cochlear amplifier at a fixed location on the BM, for increasing stapes displacement. For comparison, the passive model response, given by the amplitude (6) corresponding to (5) is given by the dashed line in Figure 1a. It is visible that deviations from the passive response only occur close to the active resonance location, and that the response peak is entirely due to active amplification.

Although the behavior of the cochlea is already very well reproduced, the experimental curves clearly display a shift of the response peak towards lower frequencies by more than 10% with increasing stimulus intensities and an associated increase in response bandwidth. The model's response shapes still increase too rapidly, followed by a flat top, and the increase in response bandwidth, as a function of the stimulus size, is too small.

### Coupled Hopf Amplifiers

If we consider the vibrating BM loaded with an array of Hopf oscillators, these oscillators must be seen as weakly coupled, which implies the possibility of coherent in-phase oscillations (Stoop et al., 2000a,b). These can generate amplification in the absence of external excitation, and, in this way, explain the emergence of spontaneous oto-acoustic emissions. Moreover, it can be expected that remaining deviations from the measured data can be removed, as models using coupling schemes among oscillators (de Boer, 1990; Geisler and Sang, 1995) show correct frequency shifts. Besides the direct coupling between the Hopf type oscillators, longitudinal coupling mediated by the (passive) BM, by means of surface tension, is a candidate that is computationally less intensive and will be considered first. The inclusion of the latter coupling is of primary interest, as it will remove the dissipation singularity at the location of resonance, and will allow to shift the peak of resonance to higher frequencies, as is required from biological measurements (see Fig. 4).

In our model, surface tension  $T(x)$  manifests itself through the dispersion relation (4), in which  $E(x)$  now has to be replaced by  $E(x) + k(x, \omega)^2 T(x)$ . Our simulations, with  $\bar{T} = 0.003$ , indeed confirm an improvement (Fig. 2). We now observe a peak shift of about 80 Hz for a stimulus frequency of 1,000 Hz. The choice of  $\mu = -200$  (before:  $\mu = -100$ ) limited the decrease in bandwidth and led to more realistic response shapes: The slopes at active resonance are now less pronounced,

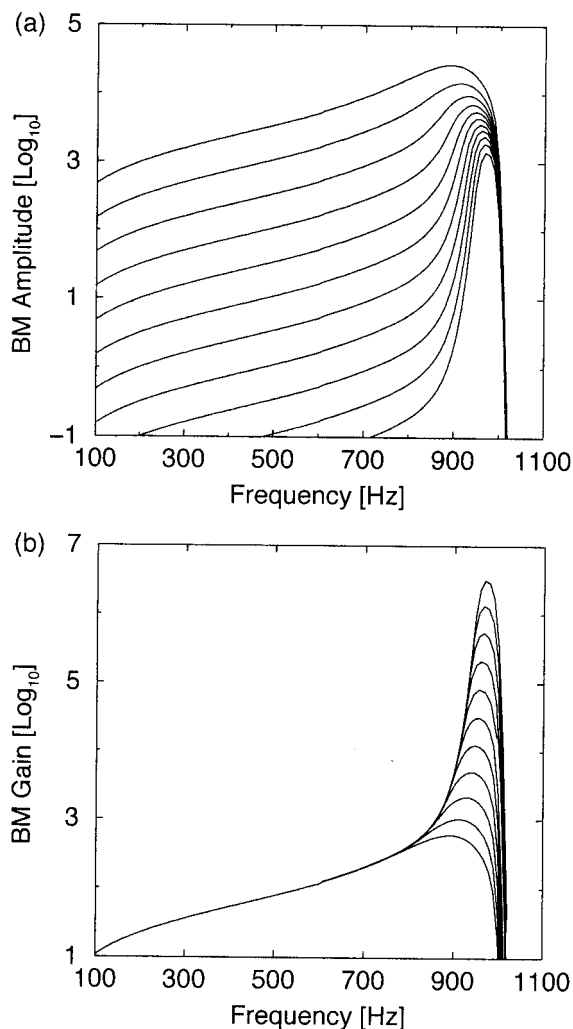


Fig. 2. BM response of the Hopf amplification model with longitudinal coupling (surface tension  $T \sim 10^{-9} E(x)$  at  $x = x_c$  (1,000 Hz), leading to  $T = 0.003$ ). **a:** Frequency response. **b:** Gain.

and the flat peaks of the simple version of our model are no longer observed.

The results still deviate from the experimental observation as the response around characteristic frequency is constant for stimuli above 60 dB (see Fig. 4). Fortunately, the direct coupling among Hopf oscillators is also suggested by anatomical findings. Micro-mechanical analysis of the arrangement of OHC's led to the conjecture that strong feed-forward coupling between the OHC exists (Geisler and Sang, 1995). We, therefore, consider feed-forward coupled OHC's as the substrate for a second mode of energy propagation  $\varepsilon(x, \omega)$  built up by the hydrodynamic wave  $e(x, \omega)$  in the vicinity of the location of active resonance. This second mode may be approximated by the integral equation

$$\varepsilon(x, \omega) = \frac{1}{\Delta x} \int_{x-\Delta x}^x H((\sigma_K(\omega)(e(x', \omega) + M\varepsilon(x', \omega)))^{1/2}), \quad (10)$$

where  $H$  is the squared amplified signal  $R$ , representing the effect of the Hopf amplifiers. The scaling parameter  $\sigma(\omega)$  is now replaced by  $\sigma_K(\omega)$ , and  $e(x, \omega)$  denotes the energy density of the hydrodynamic wave causing the BM vibration (first mode), by which the second mode is essentially driven.  $M > 0$  denotes the strength of the feed-forward coupling, which determines how fast the second mode is built up. Within the interval  $[x-\Delta x, x]$  for simplicity we choose uniform weights for all contributions to  $e(x, \omega)$ . Then the coupling to the hydrodynamic wave is given by

$$\alpha_K(e(x, \omega), x, \omega) = \frac{K_K(\omega)}{\sigma_K(\omega)} H((\sigma_K(\omega)(e(x, \omega) + F_K \varepsilon(x, \omega)))^{1/2}) \quad (11)$$

where  $F_K(\omega)$  is the coupling strength to the amplification of the hydrodynamic wave. In the differential equation (8),  $a(\cdot)$  is replaced by  $\alpha_K(\cdot)$ . With values for  $M$  and  $\Delta x$  large enough, the second mode behaves as having a kind of inertia: The accumulated (and strongly amplified) energy is gradually fed back into the hydrodynamic wave an appreciable distance beyond resonance.

In Figure 3, the amplifier responses for the optimal choice of coupling strength  $M$ , coupling range  $\Delta x$  and bifurcation parameter  $\mu$  are shown. Clearly visible effects are: (1) Increase of amplification, caused by the accumulation of energy by the coupling. (2) Shift of maximum response location (Fig. 3b), together with increased amplifier bandwidth. (3) Much stronger compressive nonlinearity around response peak and at right hand tail. (4) Compression extending to smaller  $x$  for increased amplifier input.

Frequency response and gain of the final model are shown in Figure 4, together with the experimental results. It is seen that the peak shift induced by the feed-forward coupling now amounts to about 100 Hz or 10%, which corresponds well to the experimentally observed value. The remaining discrepancies of our model from the experimental response curves (if not experimental artifacts) could be overcome by a generalization of the coupling scheme. From the obtained results, we claim that the final version of our model is able to faithfully reproduce experimentally measured BM response properties. In the present report, the results are restricted to pure tone stimuli. Examinations of the model response to complex, but still stationary, tones, thereby involving suppression phenomena and combination tone generation, are currently being performed, with excellent results.

### HOPF BIFURCATIONS AND LIMIT CYCLES IN INSECT HEARING

The hearing organs of insects are allegedly very different from those of mammals. Most prominently, the conversion of mechanical vibrations into vibrations of the cochlear fluid, with an associated matching of impedances, does not occur in insects. However, structures that look structurally similar to the mammalian cochlea do exist: For example, the sensory organ of field crickets and katydids, the crista acoustica, which resides on the forelegs, forms a linear array of cells that

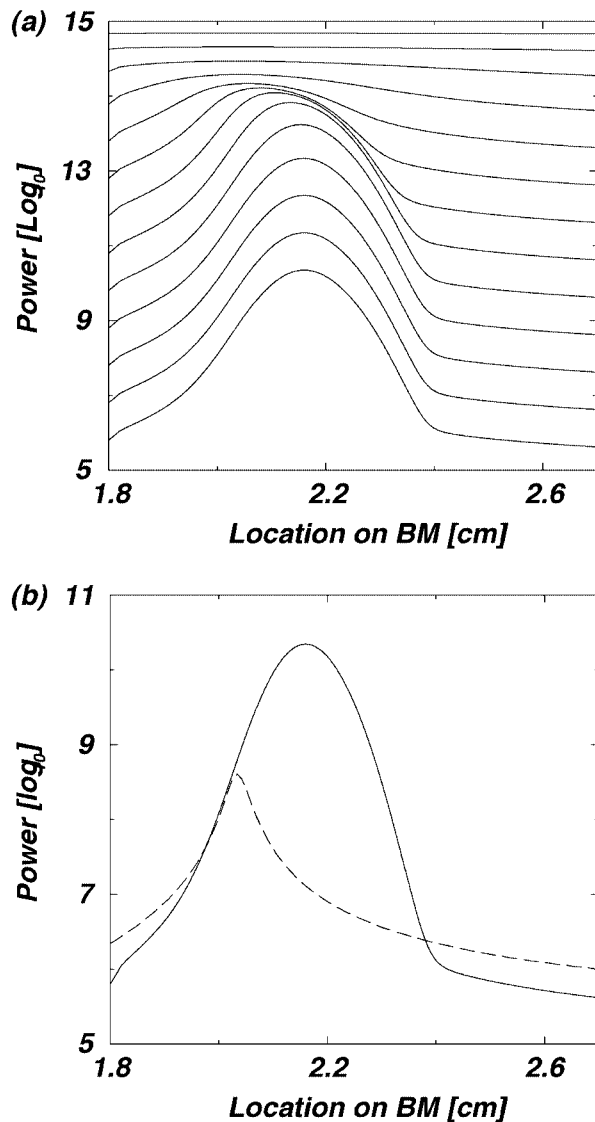


Fig. 3. **a:** Response of Hopf oscillator array with feed-forward coupling, for different input energies  $e$  from  $\{10^4, 10^5, 10^6, \dots, 10^{20}\}$ , assumed as independent from  $x$  for each curve. **b:** Response of independent (dashed) and feed-forward coupled (plain) oscillators.

is the basis for tonotopic frequency coding, which is comparable to the tonotopic map on the mammalian BM. As a consequence, the presence of oscillators and their coupling needs to be considered as potentially important experimental models.

Two principal classes of acoustic detection can be distinguished in insect audition. In close vicinity of a sound source, the sound wave consists of a bulk movement of air particles. Near-field detectors are, therefore, sensitive to particle velocity and relatively insensitive to pressure variations. *Drosophila* and mosquitoes use thin and long sensory hairs on the body or plumose antennae on the head for near-field detection. Far from a sound source, the acoustic stimulus predominantly arrives as a pressure wave. Therefore, instead of particle velocities, efficient acoustic detectors oper-

ating at a distance from a sound source are most sensitive to pressure variations. In insects, far-field detection is associated with tympanal hearing. Insect tympanal hearing organs are most diverse and can comprise only one mechanosensory cell in some moths, or up to several thousands in cicadas.

According to Robert and Hoy (1998), tympanal hearing in insects evolved from sensory organs with a proprioceptive function, for which stochastic resonance phenomena have been reported (e.g., for the cricket *Acheta domestica*; Levin and Miller, 1996). This phenomenon refers to an improved recovery of a signal when it is embedded in a (generally small amplitude) noisy background. Stochastic resonance is present if for noise of a certain nonzero amplitude, the signal-to-noise ratio attains a maximum. In a study of *Acheta domestica* (Levin and Miller, 1996), small amplitude low-frequency air disturbances that are characteristic for conspecifics or for predators, excite mechanosensory afferent neurons that synapse onto interneurons in the terminal abdominal ganglion (stimulation just suprathreshold). When a noise level of 25 times the r.m.s. amplitude of the signal is added during the presentation to the animal, the signal-to-noise ratio measured at the interneurons increases to a maximum above 8 dB, and then falls towards zero when the noise amplitude is increased.

Recent measured data (*Drosophila melanogaster*) provided by M. Göpfert and D. Robert (Göpfert and Robert, 2003) show the existence of limit cycles in insect hearing. Using laser interferometry, the mechanical behavior of the fruit fly's antenna was measured at the tip of the antennal flagellum. Spontaneous limit-cycle oscillations were observed that could also be elicited by using a chemical stimulus (DMSO, see Göpfert and Robert, 2003). Coherent temporal oscillations that can be found in the response are already a strong indicator for the presence of active amplification. When the data are further analyzed, it is seen that the typical experimental run is divided into four different temporal periods. After the application of the chemical, fast oscillations of small amplitude start to build up, that in the second time slice are fully developed, but of lower frequency. In the third time slice, the oscillation amplitudes have already decayed, with a slightly reduced frequency. In the following slice, coherent responses are absent and (possibly Brownian) noise is measured. At this point, it is likely that the cellular elements of the sensor are badly damaged. The observed oscillations are rather noisy; however, the underlying limit cycles are detectable. In order to work out these structures more properly, we applied noise-cleaning methods to the data. Already after mild noise-cleaning, the convergence of the data onto a limit cycle is evident (see Fig. 5). From further analysis using fractal dimensions and Lyapunov exponents, we conclude that the variability that can be observed in the data is not of a chaotic nature, but of a noisy, stochastic nature. Whereas the original data yield a positive largest Lyapunov exponent (about 0.08), when the data is mildly noise-cleaned, this exponent is reduced to less than half that figure, which indicates that no coherent separation of trajectories exists. This means that the largest exponent is noise-generated and not chaotic. After noise-cleaning, the modified data were compared to the

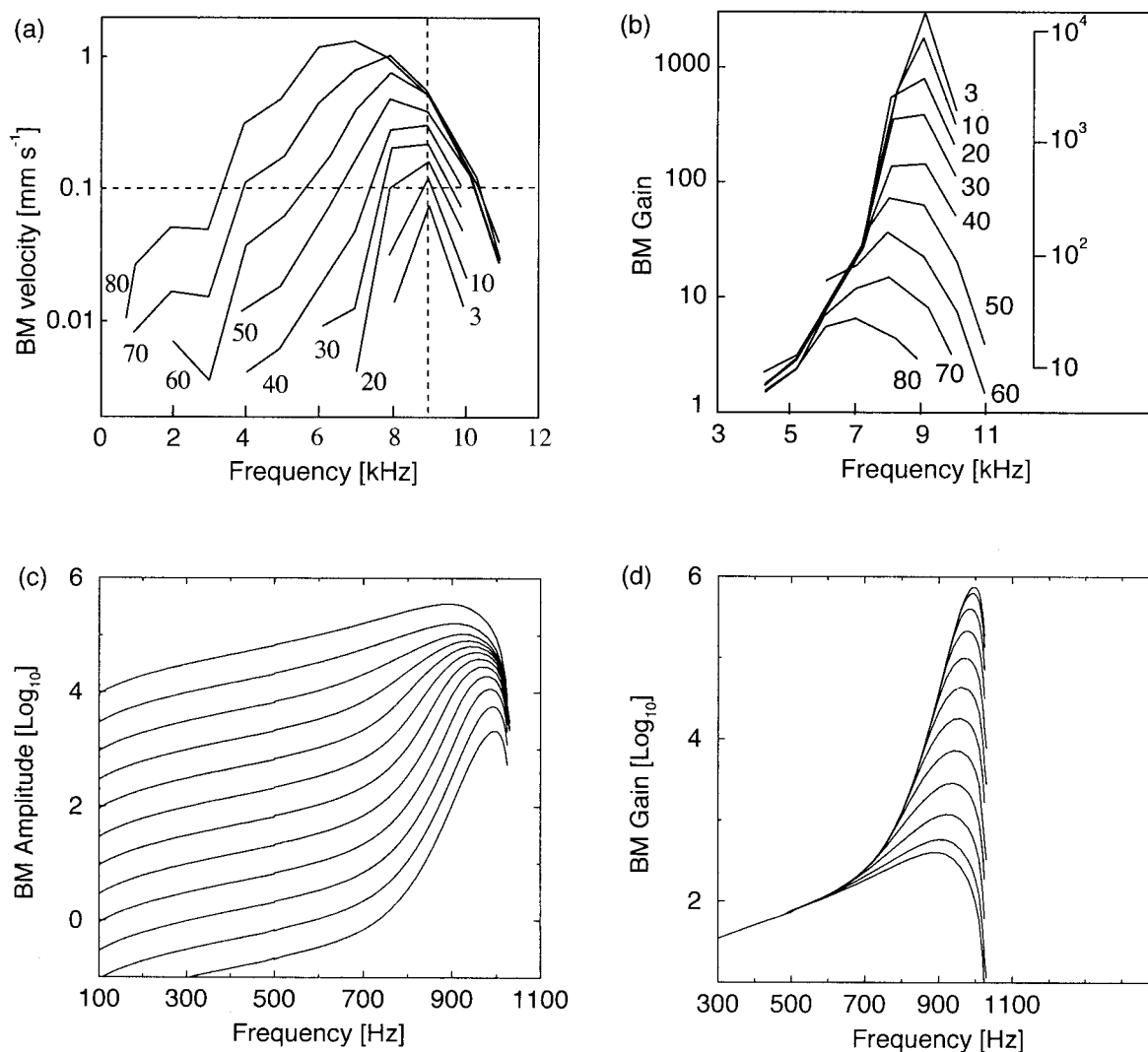


Fig. 4. Cochlear response with longitudinal feed-forward coupling of Hopf oscillators. **a:** Experimentally obtained BM frequency response (adapted from Ruggero, 1992). **b:** Experimentally obtained BM gain. **c:** Model frequency response. **d:** Model gain.

original data. Using a BDS-test, it was ensured that artificial information was not added by the noise cleaning, nor was existent information destroyed. The final conclusion from the analysis is that the data can be well approximated by a limit cycle in dimension 5. From the perspective of auditory function, this suggests the existence of a mechanism of active amplification, and that the generation of amplification is of a low-dimensional nature, with a dimension close to those measured in the mammalian cortex (e.g., the cat's visual cortex V1; Stoop et al., 2002).

These considerations fuel the need for further questions pertaining to the nature of the oscillators involved. The general experimental accessibility of the auditory system in insects may make it possible to unveil the physical nature and the physiological processes constituting these oscillators. Under which conditions do nonlinear oscillators emerge and what char-

acteristic physical and biological properties can be expected from coupled nonlinear oscillators?

### NOISE AND LIMIT CYCLES

The earliest theoretical explanations of the phenomenon of stochastic resonance were in the context of perturbations of a limit cycle, where it is easy to observe (Derighetti et al., 1985; Wiesenfeld and McNamara, 1985). In biological applications, noise can be imagined to drive a limit cycle, for which the signal acts like a perturbation. However, more recent investigations, including one on holographic synapses (Stoop et al., 2003), underline that the effect is very general. Holographic synapses (a lesser known mathematical abstraction of biological neurons), can be used for pattern recognition. They show best performance, if noise is added to the input signal. Also in this case, at the heart of the phenomenon is an averaging process,

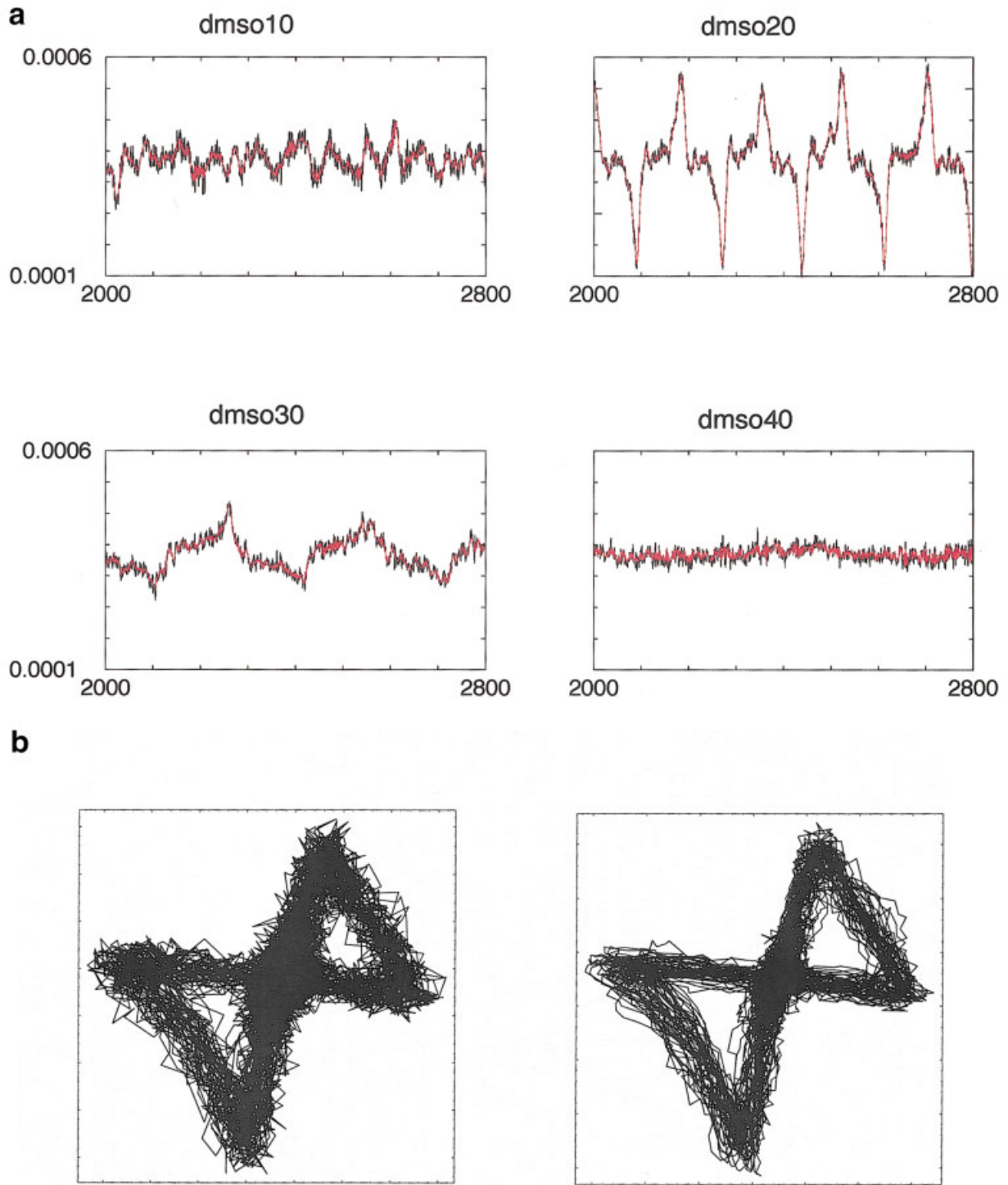


Fig. 5. Limit cycles from insect hearing (*Drosophila melanogaster*). **a:** Response measured in the different response slices, revealing in each time very strong noise fluctuations, which using noise-cleaning, were partially removed. Black: original data. Red: Noise-

cleaned data. **b:** Effect of noise cleaning for time-slice 2. The original data is very noisy (**left**). Mild noise cleaning improves the limit cycle nature of the oscillations, where structures indicating possible chaotic behavior are absent (**right**, embedding dimension  $d_E = 16$ ).

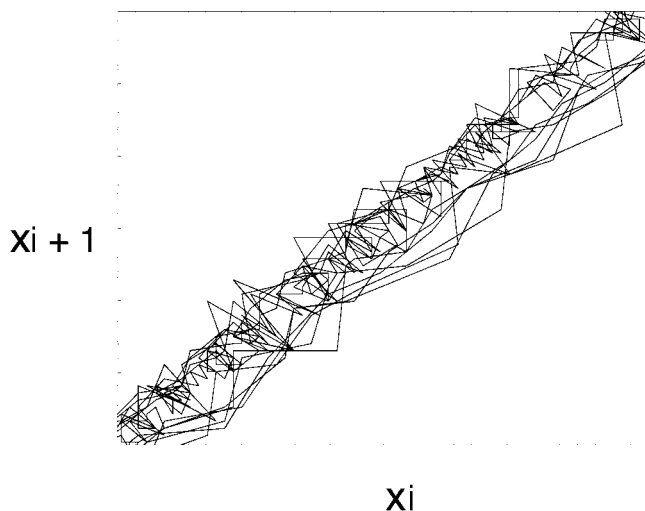


Fig. 6. In vitro random walk (resulting in regular firing). This system can be modeled by a one-sided quasi-one-dimensional random walk with a drift towards the firing threshold. The limit cycle behavior is just a mathematical mesoscopic description of this situation.

where effects disturbing the discrimination of signals are averaged out.

Although insects have fewer neurons than mammals, their mostly comparable physiology can be expected to work in comparable ways. From in vivo measurements of cortical neurons in vertebrates, it becomes evident that two classes of neurons exist (Stoop et al., 2002): One group fires in a random fashion, whereas the other group exhibits, in some cases, very stable firing patterns. Moreover, it appears that neurons firing in patterns respond with pattern-sharpened firing when driven by the optimal stimulus. A neuron has a variable number of synaptic contacts, often as many as 10,000 (Abeles, 1982). If each individual input appears in an incoherent fashion and has about equal weight, depending on the average activity of this pool, their average will amount to a quasi-constant driving current that slowly varies along with the average activity. If the input is larger than the loss associated with the decay of the membrane potential, the neuron will start to fire in a regular fashion, and only if little adaptation is present. However, firing of neurons has been observed to be highly variable, much more than could be expected from the situation depicted above. Several different models have been proposed but the issue of firing variability remains unresolved.

Shadlen and Newsome (1994) compared three models of synaptic integration, distinguished according to the number  $n$  of synaptic inputs needed for spike activation (scaled by time), where they used Poisson-distributed input (a somewhat arbitrary assumption), giving rise to a random walk similar to the one in Figure 6. Integrate and fire neurons, with  $n = 300$ , show clock-wise regular firing, due to the central limit theorem (e.g., Feller, 1971). Coincidence detector neurons asking for  $n = 35$  synaptic inputs within 1 ms to fire, fire rather variably, albeit at a somewhat increased mean membrane potential. Neurons requiring for firing  $n = 25$  excitatory events above resting potential in

a balanced inhibitory-excitatory network also achieve a large degree of variability, where it has been claimed that the network activity is chaotic.

In general, the simplest cortical in vitro preparations lead to regular firing behavior. In vivo measurements (anesthetized preparation, visual stimulation), however, show two broad classes of neurons: One with low-dimensional firing properties, and another with stochastic/noisy firing characteristics. Therefore, going from the in vitro to the in vivo situation encompasses a qualitative and a quantitative increase towards chaotic behavior of the involved neurons.

To bring a neuron to chaotic firing, there are three possibilities.

1. A neuron can become chaotic if it has relatively strong interaction with other chaotic neurons.
2. As a biological neuron is a device acting within a limited working range, it can be exhibiting a strongly nonlinear behavior. It is generic that such devices, when driven hard enough, will respond with chaotic behavior. Therefore, internal strongly nonlinear interaction, e.g., of ion currents, could bring neurons into chaotic firing. It seems that in the well-investigated neural network of the gastrosomatic ganglion of crayfish, such behavior has been observed (A. Selverston, private communication).
3. The last possibility has been discussed in the literature to a very small extent. It is the question of how stable the external inputs can be assumed to be, especially in the in vivo condition. If the driving activity is varying in a chaotic fashion, the individual neurons' firing behavior will very likely follow this behavior, especially since we can assume that for certain stimulations, different cortical circuits will become active, which will lead to a strong separation property within the network. It can even be imagined that under relatively stable external conditions, interaction between different sensory cortical subsystems may generate a chaotic interplay, possibly driven by the non-occurrence of final actions in the anesthetized animal.

We would like to point out that, if the neuron fires chaotically, the firing should be composed from fundamental patterns hidden within chaos. Furthermore, as we will expect the activity to be driven externally, the patterns have to be rescaled to standard activity. Otherwise, possible chaotic behavior will be mistaken as stochastic (unfortunately, an analysis distinguishing between both behaviors seems not to have been performed). Chaos has some advantages over stochastic behavior: It is composed of different patterns that may lead to well-defined actions in the population. These patterns can be unstable, if supplemented by a controlling device, or marginally stable, if input-driven. In either case, the advantages this property has is that of fast adaptability, and that it enables the (potentially very stable) synchronization of ensembles of unstable patterns.

For insects, ensembles of neurons of the size required by the third scenario seem not to exist, and different justifications for inhibitory neurons from balanced networks can be given (e.g., increased potential for synchronization). We will, therefore, describe how an in-

tegrating neuron can become chaotic according to the first scenario. When a neuron only obtains a small amount of noisy, uncorrelated input, it will remain in equilibrium. Upon sufficient sustained input, however, it will enter a state of regular oscillation—a bifurcation has taken place. If the oscillation onset is abrupt, starting at a frequency remote from zero, the bifurcation is called hard or subcritical; if its onset is continuous, it is called soft or supercritical. Whereas hard Hopf bifurcations are typically generated from coupled nonlinear differential equations [e.g., FitzHugh-Nagumo equations (FitzHugh, 1961), experimentally: non-adapting interneurons], soft Hopf bifurcations can emerge from simpler systems as one parameter changes. Moreover, an effect similar to a soft Hopf bifurcation is generated by a saddle-node bifurcation. In this case, regular firing with an arbitrarily low frequency can be achieved, as is observed, e.g., for pyramidal cells in the cortex.

Whereas the non-spiking neuron behavior is associated with a (stable) fixed-point of the equations describing the system's evolution, regular firing by neurons is usually associated with the mathematical model of a limit cycle. Stable fixed-points are attracting with respect to perturbations in all possible directions (as many as the algebraic dimension of the evolution equation indicates). After the bifurcation, all but one direction are still attractive: Along the motion, the stability has become neutral. How can, from this regular firing behavior, chaotic patterns emerge? In Shadlen and Newsome's (1994) simulations, only synaptic contacts of the same size and strength were taken into account, which is a strongly artificial setting. It has been observed that synapses undergo long-term synaptic potentiation and depression, respectively, depending on the time at which the pre-synaptic spike arrives at the post-synaptic neuron, with respect to its own spike. As a consequence, what a neuron receives as input is much more precisely described by the following scheme:

- *Small-scale input* (e.g., from remote synapses) drives the neuron towards regular spiking with well-defined periodicity. This small-scale input will be referred to as noisy input. Note that such a type of input is able to reflect local gradients of excitation in the network
- *Strong input* from next neighbors (neurons or a group of synchronized neurons)
- *Medium-size interactions* that may reflect specific conditions in the neighborhood of the neuron, transmitted most likely by interneurons

As small-scale input will drive the neuron into limit-cycle firing behavior, the question is how these objects interact under strong exchange of perturbations. If limit cycles interact, it is in a generic way. Generically, they will have incommensurable firing frequencies (with irrational frequency  $\Omega = f_0/f_s$ , where  $f_0$  is the frequency of the target and  $f_s$  is the frequency of the perturbation) as there are abundantly more irrational than rational numbers in the unit interval. When, however, the coupling is activated, with a strength measured by  $K$ , neuron pairs start to lock their firing in rational frequency ratios, which naturally give rise to the notion of periodicity. As  $K$  is increased further,

neurons with dissimilar firing frequencies are recruited by different locked frequencies at the same time. As a consequence, chaotic firing behavior of the neurons is observed.

The outlined paradigm was experimentally verified for cortical neurons (Stoop et al., 2000a): A neuron was driven by a constant input current to regular firing. From an afferent nerve, a regular stimulation signal was applied, closely resembling pre-synaptic neuronal signals. As a result, the postsynaptic neuron locked its firing behavior to the frequency of the stimulation. Investigation of the returned periodicities  $p$  as a function of  $\{\Omega, K\}$  results in typical Arnol'd tongue structures (e.g., Glass and Mackey, 1988) (see Fig. 7 and 8). For each periodicity  $p$  there are different "tongues," which comprise areas in the  $\{\Omega, K\}$ -parameter space having solutions of the same periodicity  $p$  and same effective (locked) rational frequency. Note that all periodicities appear, according to the Farey-tree, but with ever smaller basins of attraction. For the different areas, the stability properties of the solutions, which are measured by the *Lyapunov exponent*  $\lambda(\Omega, K)$ , are of interest.

Zooming in on the Arnol'd tongues reveals that for inhibition, chaotic behavior is possible ( $\lambda(\Omega, K) > 0$ ; Peinke et al., 1992), at least from the numerical point of view. However, relatively large input strengths are needed to generate this response. Analytic investigations prove that chaotic behavior indeed occurs on a set of non-zero Lebesgue measure in the relevant parameter space (Stoop et al., 2000b). This is the area where chaos of the first scenario can be generated. The results obtained for binary interaction generalize to higher  $n$ -ary interaction, for which similar results can be obtained (see Baesens et al., 1991).

That biological neurons are indeed on limit cycle solutions has been shown experimentally: When the frequency ratio is changed, firing along the Farey-tree is found (Stoop et al., 2000a). This is the (first) experimental proof that biological neurons, when stimulated by a constant current, are on limit cycles.

### ENCODING OF INFORMATION BY LIMIT CYCLES

In order to see what coupling of limit cycles can contribute towards a better understanding of neuronal activity, we focus on a code that is intrinsic to the Arnol'd tongues. A code is a partition of a usually continuous physical phase-space of the evolving system into areas that then are symbolically labeled, for example, by some letters. Each time the system's trajectory enters a specific area of the phase-space, the associated letter is reported. The code is useful if it succeeds in the discrimination of states in an unambiguous way up to a chosen precision by a symbol sequence of sufficient length. Our coding system consists of a small number (say: 2) of coupled noise-driven limit cycles. The noise level and the two excitabilities then fully describe the system. Alternatively, these inputs are coded by the periodicity of the spiking of the targeted neuron and by its spiking frequency. Schematically, we may, therefore, write:

$$\{f_1, f_2\} \rightarrow \{p, f_2\}, \quad (12)$$

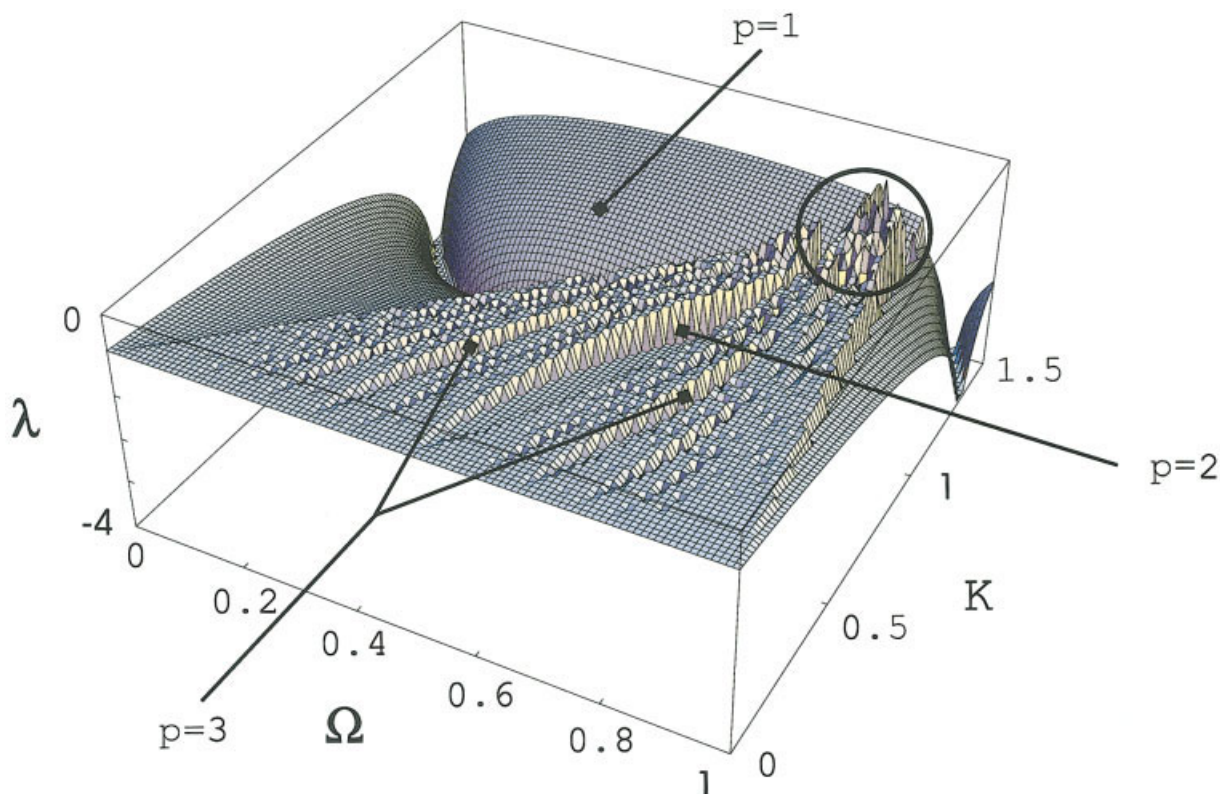


Fig. 7. Lyapunov exponents indicate the stability of the emerging response for inhibitory binary neuron interaction, on the natural parameter space. Higher Lyapunov exponents indicate less stability. Observe the emergence of the so-called Arnol'd tongues (scars in the plot). On each scar, the periodicity  $p$  of the perturbed neuron's response is fixed (partially exemplified in the figure). The more stable

the neuron's response, the lower generally is  $p$ . The circle indicates the location where chaotic response occurs. A similar result is obtained for excitation. However, excitation fails to reach the region associated with chaotic behavior (the cell cannot sustain such strong excitatory inputs and dies).

where  $f_1$  is the frequency of the perturbing neuron and  $p$  labels the periodicity. How this coding scheme is experimentally observed is shown in Figures 7 and 8. It is now worth emphasizing the special properties of this code. It is a code that is

- robust towards adaptation and relaxation processes
- independent of the excitability level in homogeneously excited area, in the sense that  $\Omega = f_1/f_2$  remains fixed, but only responds to local gradients of the noise level
- nearly optimal: higher probabilities correspond to lower periodicities (likewise to the Huffman code; e.g., Ash, 1965)
- able to code phase-coding as well as frequency-coding.

To illustrate the last point we emphasize that

- phase-coincidence essentially triggers an increase of  $K$ .
- frequency-coded input to the neuron essentially changes  $\Omega$

The result of the interaction between the two neurons can be seen as a computation, as it drastically

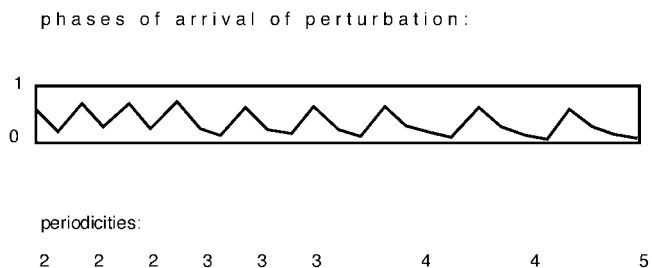


Fig. 8. Evolution of the locking between two neurons as one firing frequency, and consequently  $\Omega$ , is changed (from 0.75 to 0.9), but  $K$  is held constant at  $K = 0.85$ . Experimental data (rat somatosensory barrel cortex, pyramidal neurons). The periodicity evolves exactly according to the prediction by the Farey-tree, proving that the experimental neurons are indeed on limit cycle solutions.

decreases the potentially accessible forms of spike trains. Moreover, the result of this computation can be read out from a third neuron. The interesting observation here, of course, is that the result of the computation is interpreted in different ways, according to the state of the read-out neuron (where in the state again information is contained). Figure 9 illustrates this point.

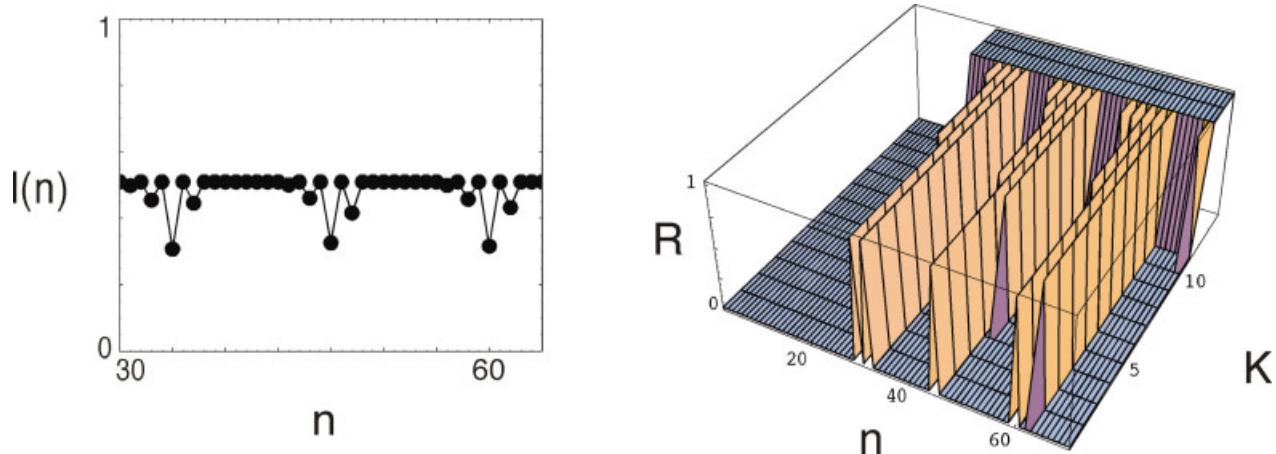


Fig. 9. Read-out neuron. **Left:** Input signal. Displayed is the  $n$ 'th interspike interval as a function of  $n$ . **Right:** Response by the read-out neuron as a function of its excitability. The read-out neuron is mod-

eled by a constant level of activity ("excitability") and an exponential decay towards this state for strong perturbations. At low excitability, only fast successions of input spikes trigger a firing event.

How important is locking in extended neural networks? Even in the simplest nearest neighbor neuronal networks based on measured perturbation profiles and firing frequencies of rat barrel cortex pyramidal neurons, mild self-organized activities emerge. For the individual neuron, this leads to small oscillations around the mean firing frequency. For appropriate neighboring neuronal activities, even in this quasi-stationary setting, locked neuronal firing can be observed, albeit slowly modulated by the underlying network oscillation. In Figure 10, two typical responses from this model are shown. At the site illustrated (Fig. 10, left), the influence by the network is so strong that no coherent response to the stimulation by the neighboring sites is found. In contrast, the response is locked at the site (Fig. 10, right) (period 8). One interpretation of these results is the following: More strongly coupled clusters can be relatively stable, if the network modulation does not change the internal relations between neurons too much. When the network activity induces a time-varying competition among the neighboring neurons, the considered neuron will fall from one locked state into another, which leads to firing in an erratic manner. In terms of the observations made previously, the set of neurons falls into two classes: Neurons that perform temporally stable computations, in contrast to neurons that are not firing in a coherent fashion. The latter nevertheless may transmit information by means of their firing frequency. According to the principles of synaptic potentiation and depression, they, however, will target mostly weakly coupled neurons.

### Driving Locked States Generate Large Variability

Is there any supporting indication for the proposed way of information processing? Below, we sketch two scenarios that might be a consequence of the proposed encoding. Although endowed with appealing mathematical properties, locked states are seldom observed in *in vivo* neuronal firing, where the closest findings are from hippocampal place cells. An explanation of the

difficulty of observation can be given on the basis of the following arguments. External sensory input or internal collective spatio-temporal self-organization may lead to a strong driving of the neural activity. The essential observation now is that locked states can persist under strong driving, if their firing frequency is relationally affected by the driving. This is the case, whenever the condition  $\Omega = f_1(t)/f_2(t) = \text{const}$  is met. From the computational point of view, this indicates that the relationship between the neurons has not been changed, hence an unchanged result of computation is returned. The response, however, will not be recognized as locked, since the driving affects the time axis similarly to a nonlinear transformation. As we are used to measure locking by assuming a homogeneously scaled time axes, and normally do not rescale by activity, we are generally unable to recognize locked responses under dynamic driving conditions. Figure 11 illustrates this observation, where driving, spike train, and activity-rescaled phases of perturbations are shown.

As a result, we propose the following interpretation of the behavior of biological noise-driven cortical networks:

1. Locked neuron firing is a simple, emergent way of expressing local neuronal computation. While for weak local interaction the local spiking behavior is dominated by a wealth of different periodicities, for stronger interaction, there is a tendency for the response to settle towards more simple and more stable spiking patterns.
2. In the quasi-stationary case, locally, low-periodic locked spiking behavior may be expected in abundance. This periodic response is organized along Arnol'd tongues.
3. In the case of strong driving of the network, these lockings may persist, but will be difficult to observe.
4. These "regular" spiking patterns are in sharp contrast to local chaotic response, which exists for strong inhibition on a nonzero Lebesgue measure of the parameter space. The latter expresses that

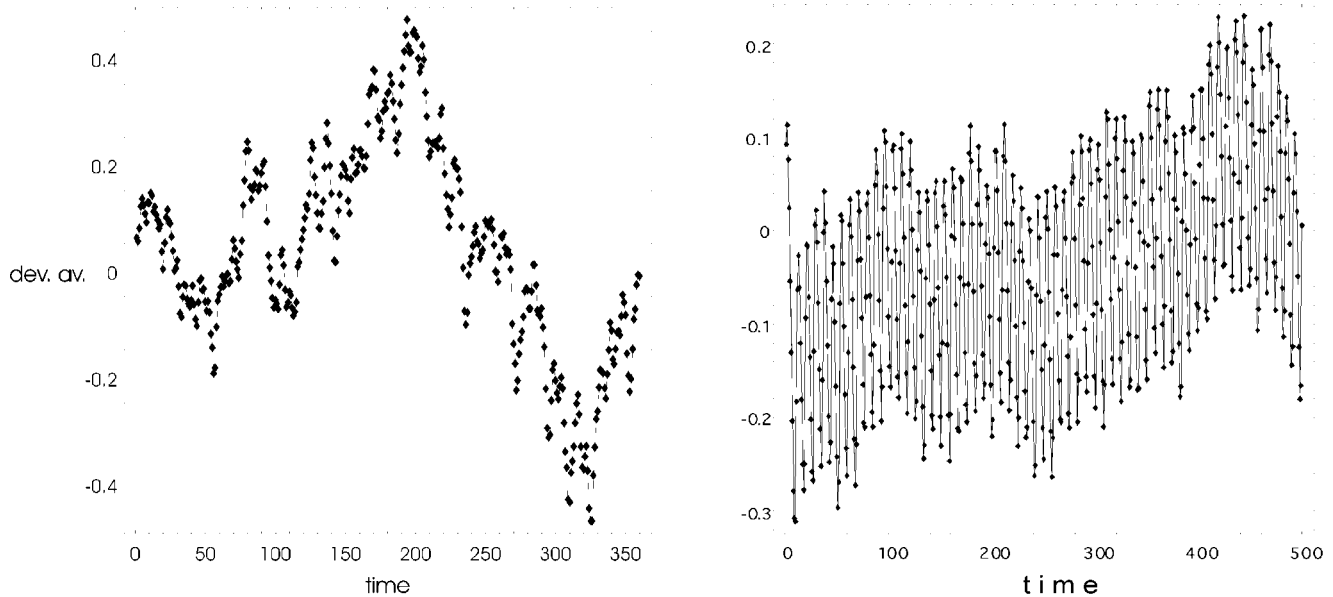


Fig. 10. 2-d next neighbor network, with interaction based on measured perturbation profiles (pyramidal neurons of barrel cortex). **Left:** Incoherent neuronal firing, dominated by long-range network effects. **Right:** Embedded locked neuronal firing (period 8).

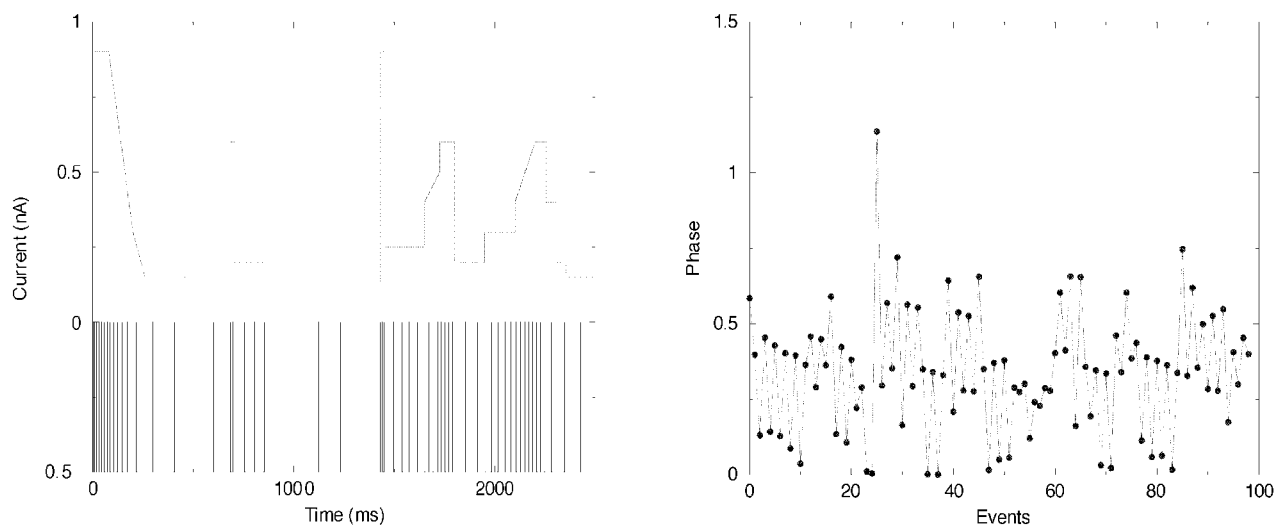


Fig. 11. **Left:** Driving current and spike train of by external activity driven, in period-2 interacting limit cycle neurons (simulation). **Right:** Phases, when the driving is transformed away, indicating that period-2 persists.

chaos should be observable, or that systems could be tuned to this state. It is noteworthy that chaos requires comparatively strong local coupling, and occupies only a small portion of the parameter space. Local chaotic response enables synchronization among different neuronal ensembles.

5. This form of chaos, however, needs to be distinguished from more global, spatio-temporal chaos, which is generated by chaotic driving, either by sensory input or by principles of self-organization.

We propose that locking plays a role similar to the unstable periodic orbits in chaotic systems (Grebogi et al.,

1988). It provides the backbone for the complex structure hidden in the seemingly intractable chaotic motion.

#### Long-Tailed Interspike Interval Distributions: Indicators for Driving by Activity

It is usually assumed that interspike interval distributions are described by Poissonian probability distributions. In states of quasi-equilibrium brain activity, we may reasonably expect neurons to be close to marginally stable states. From these states, however, interspike distributions governed by Lévy-type probability laws emerge. In near-to-equilibrium states, neurons change their perturbation partners quite randomly, probably suf-

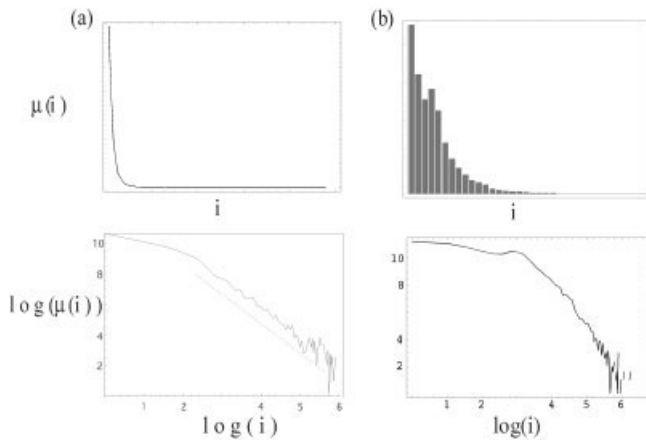


Fig. 12. Interspike interval distributions from cat striate cortex recordings (see text). **a:** A fine grating, resulting in a smooth probability distribution. **b:** Using a coarser grating shows the “second frequency” predicted by the model. The corresponding log-log scale plots show an almost perfect power-law for (a) (indicated by a line), in contrast to (b).

fering from a (log-normal) random number of inhibitory and excitatory perturbations between the spikes. Implementing this point of view in a simulation, we indeed observed perfect power-law decay behavior, superimposed by self-similar structures (e.g., Teich, 1992), that are most prominent for strong local activity (large local K-values). We checked this understanding against an experiment in which we recorded neuron spiking activity in cat striate cortex. Anesthetized cats were shown isotropic random point patterns with varying granularities, moving in the preferred direction of the observed neuron (e.g., Ahmed et al., 1997). A reasonable assumption is that the excitability K directly corresponds to the coarseness of the point pattern. Indeed, our experimental observations verify these predictions (see Fig. 12). From our sample of 11 files comprising between 2,000–15,000 spikes, 9 files showed clear power-law behavior, while two were probably not asymptotic enough.

## CONCLUSIONS

Using the example of a novel model of cochlear hearing, we have reviewed and presented new evidence for the importance of limit cycles in audition. We elucidated the universality properties of these objects and presented illustrative data, though most of them not directly connected with hearing. A generic model for information processing in noisy environments was proposed. In this model, comparing analog signals results in a digital output, the periodicity. In addition to contributing to a general understanding of audition and its active components, the evidence presented here also sheds some light onto the co-existence between order and noise in neural systems, and on the origin of chaotic behavior.

## REFERENCES

Abeles M. 1982. Local cortical circuits. Berlin: Springer.  
 Ahmed B, Allison JD, Douglas RJ, Martin KAC. 1997. An intracellular study of the contrast-dependence of neuronal activity in cat visual cortex. *Cereb Cortex* 7:559–570.  
 Ash RB. 1965. Information theory. London: Dover.

Baesens C, Guckenheimer J, Kim S, MacKay RS. 1991. Three coupled oscillators: mode-locking, global bifurcations and toroidal chaos. *Physica D* 49:387–475.  
 Crawford A.C., Fettiplace R. 1983. An electrical tuning mechanism in the turtle cochlear hair cells. *J Physiol* 312:377–412.  
 de Boer E. 1980. Auditory physics. Physical principles in hearing theory I. *Phys Rep* 62:87–174.  
 de Boer E. 1990. Auditory physics. Physical principles in hearing theory III. *Phys Rep* 203:125–231.  
 Derighetti B, Ravani M, Stoop R, Meier PF, Brun E, Badii R. 1985. Period doubling lasers as small-signal amplifiers. *Phys Rev Lett* 17:1746–1749.  
 Eguíluz VM, Ospeck M, Choe Y, Hudspeth AJ, Magnasco MO. 2000. Essential nonlinearities in hearing. *Phys Rev Lett* 84:5232–5235.  
 Feigenbaum M. 1978. Quantitative universality for a class of nonlinear transformations. *J Stat Phys* 19:25–52.  
 Feller W. 1971. An introduction to probability theory and its applications. Vol. 2. New York: John Wiley.  
 FitzHugh R. 1961. Impulses and physiological states in models of nerve membrane. *Biophys J* 1:445–466.  
 Geisler CD, Sang C. 1995. A cochlear model using feed-forward outer-hair-cell forces. *Hear Res* 86/1,2:132–146.  
 Glass L, Mackey M. 1988. From clocks to chaos. Princeton: Princeton University Press.  
 Gold T. 1948. Hearing. II. The physical basis of the action of the cochlea. *Proc R Soc Lond B* 135:492–498.  
 Göpfert MC, Robert D. 2003. Motion generation by *Drosophila* mechanosensory neurons. *Proc Natl Acad Sci USA* 100:5514–5519.  
 Grebogi C, Ott E, Yorke JA. 1988. Unstable periodic orbits and the dimensions of multifractal chaotic attractors. *Phys Rev A* 37:1711–1724.  
 Helmholtz HLF. 1863. Die Lehre von den Tonempfindungen. Braunschweig: Vieweg.  
 Hopf E. 1942. Abzweigung einer periodischen Lösung von einer stationären Lösung eines Differentialgleichungssystems. *Ber Math-Phys Sächs Akad d Wiss Leipzig* 94:1–22.  
 Kemp DT. 1978. Stimulated acoustic emissions from within the human auditory system. *J Acoust Soc Am* 64:1386–1391.  
 Kern A, van der Vyver J-J, Stoop R. 2002. Towards a biomorphic silicon Hopf cochlea. Proceedings of the NDES IEEE conference on nonlinear dynamics of electronic systems. p 2-1–2-4.  
 Levin JE, Miller JP. 1996. Stochastic resonance enhances neural encoding of broadband stimuli in the cricket cercal sensory system. *Nature* 380:165–168.  
 Lighthill J. 1981. Energy flow in the cochlea. *J Fluid Mech* 106:149–213.  
 Martin P, Hudspeth AJ, Jülicher F. 2001. Comparison of a hair bundle’s spontaneous oscillations with its response to mechanical stimulation reveals the underlying active process. *Proc Natl Acad Sci USA* 98:14380–14385.  
 Patuzzi R. 1996. Cochlear micromechanics and macromechanics. In: Dallos P, Popper AN, Fay RR, editors. *The cochlea*. New York: Springer. p 186–257.  
 Peinke J, Parisi J, Roessler OE, Stoop R. 1992. Encounter with chaos. Berlin: Springer.  
 Robert D, Hoy RR. 1998. The evolutionary innovation of tympanal hearing in Diptera. In: *Comparative hearing: Insects*. New York: Springer.  
 Ruggero MA. 1992. Response to sound of the basilar membrane of the mammalian cochlea. *Curr Opin Neurobiol* 2:449–456.  
 Shadlen MN, Newsome WT. 1994. Noise, neural codes and cortical organization. *Curr Opin Neurobiol* 4:569–579.  
 Stoop R, Schindler K, Bunimovich LA. 2000a. When pyramidal neurons lock, when they respond chaotically, and when they like to synchronize. *Neurosci Res* 36:81–91.  
 Stoop R, Schindler K, Bunimovich LA. 2000b. Neocortical networks of pyramidal neurons: from local locking and chaos to macroscopic chaos and synchronization. *Nonlinearity* 13:1515–1525.  
 Stoop R, Blank DA, Kern A, van der Vyver J-J, Christen M, Lecchini S, Wagner C. 2002. Collective bursting in layer IV: synchronization by small thalamic inputs and recurrent connections. *Cog Brain Res* 13:293–304.  
 Stoop R, Buchli J, Keller G, Steeb W-H. 2003. Stochastic resonance in pattern recognition by a holographic neuron model. *Phys Rev E* 67:061918.1–061918.6.  
 Teich M. 1992. Fractal neuronal firing patterns. In: McKenna T, Davis JL, Zornetzer SF, editors. *Single neuron computation*. San Diego: Academic Press. p 589–625.  
 von Békésy G. 1960. Experiments in hearing. New-York: McGraw-Hill.  
 Wiesenfeld K, McNamara B. 1985. Period-doubling systems as small-signal amplifiers. *Phys Rev Lett* 55:13–16.